

OAK RIDGE NATIONAL LABORATORY LIBRARIES



3 4456 0551783 9

ORNL/TM-7255

ornl

OAK
RIDGE
NATIONAL
LABORATORY

UNION
CARBIDE

Crack Propagation in Hastelloy X

T. Weerasooriya
J. P. Strizak

OAK RIDGE NATIONAL LABORATORY
CENTRAL RESEARCH LIBRARY
CIRCULATION SECTION
4500N ROOM 175

LIBRARY LOAN COPY

DO NOT TRANSFER TO ANOTHER PERSON

If you wish someone else to see this
report, send in name with report and
the library will arrange a loan.

UCN-7969 (3-9-77)

OPERATED BY
UNION CARBIDE CORPORATION
FOR THE UNITED STATES
DEPARTMENT OF ENERGY

Printed in the United States of America. Available from
National Technical Information Service
U.S. Department of Commerce
5285 Port Royal Road, Springfield, Virginia 22161
NTIS price codes—Printed Copy: A03 Microfiche A01

This report was prepared as an account of work sponsored by an agency of the United States Government. Neither the United States Government nor any agency thereof, nor any of their employees, makes any warranty, express or implied, or assumes any legal liability or responsibility for the accuracy, completeness, or usefulness of any information, apparatus, product, or process disclosed, or represents that its use would not infringe privately owned rights. Reference herein to any specific commercial product, process, or service by trade name, trademark, manufacturer, or otherwise, does not necessarily constitute or imply its endorsement, recommendation, or favoring by the United States Government or any agency thereof. The views and opinions of authors expressed herein do not necessarily state or reflect those of the United States Government or any agency thereof.

ORNL/TM-7255
Distribution
Category UC-77

Contract No. W-7405-eng-26

METALS AND CERAMICS DIVISION

HTGR BASE TECHNOLOGY PROGRAM

Fueled Graphite Development (189a 01330)

CRACK PROPAGATION IN HASTELLOY X

T. Weerasooriya and J. P. Strizak

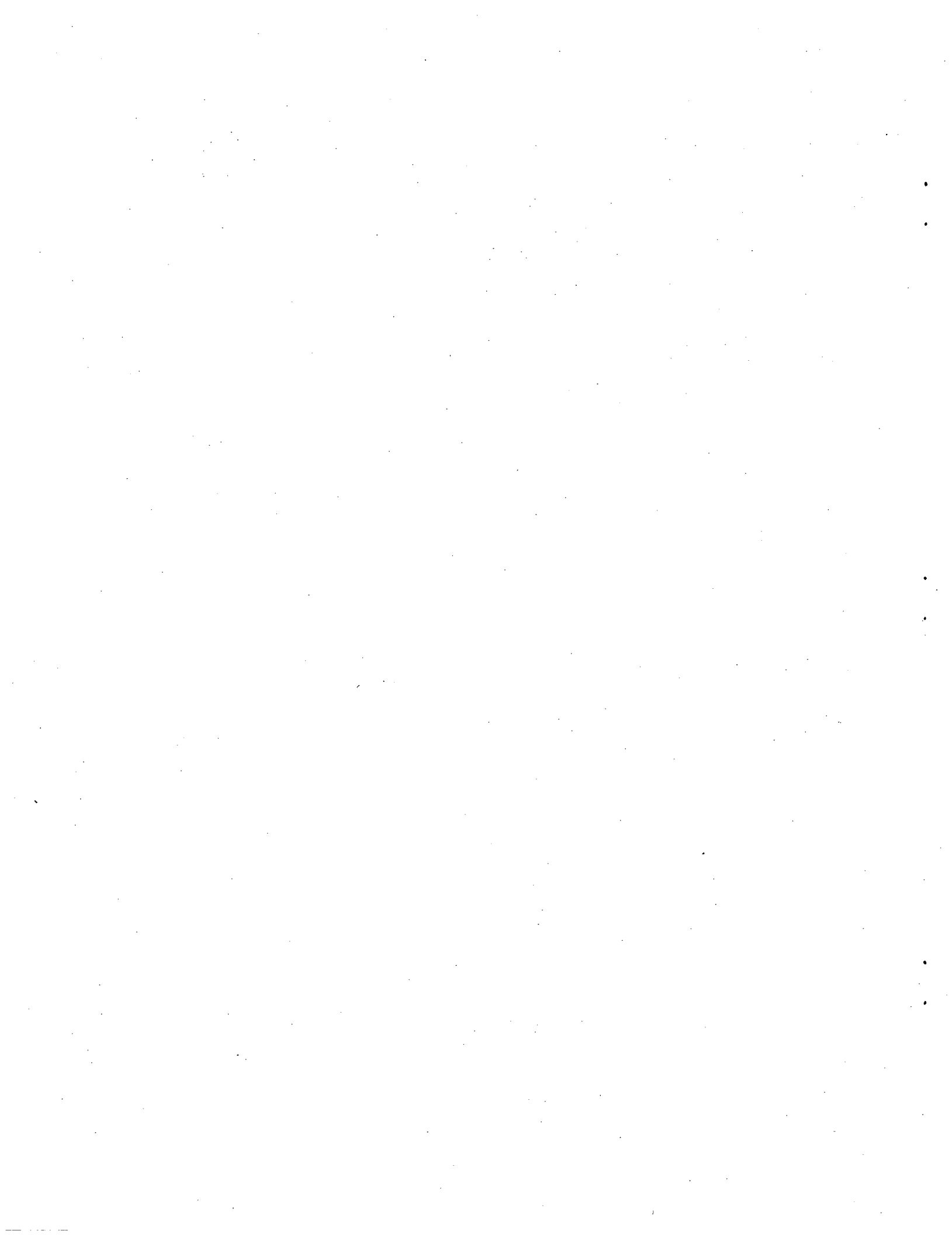
Date Published: May 1980

OAK RIDGE NATIONAL LABORATORY
Oak Ridge, Tennessee 37830
operated by
UNION CARBIDE CORPORATION
for the
DEPARTMENT OF ENERGY

OAK RIDGE NATIONAL LABORATORY LIBRARIES

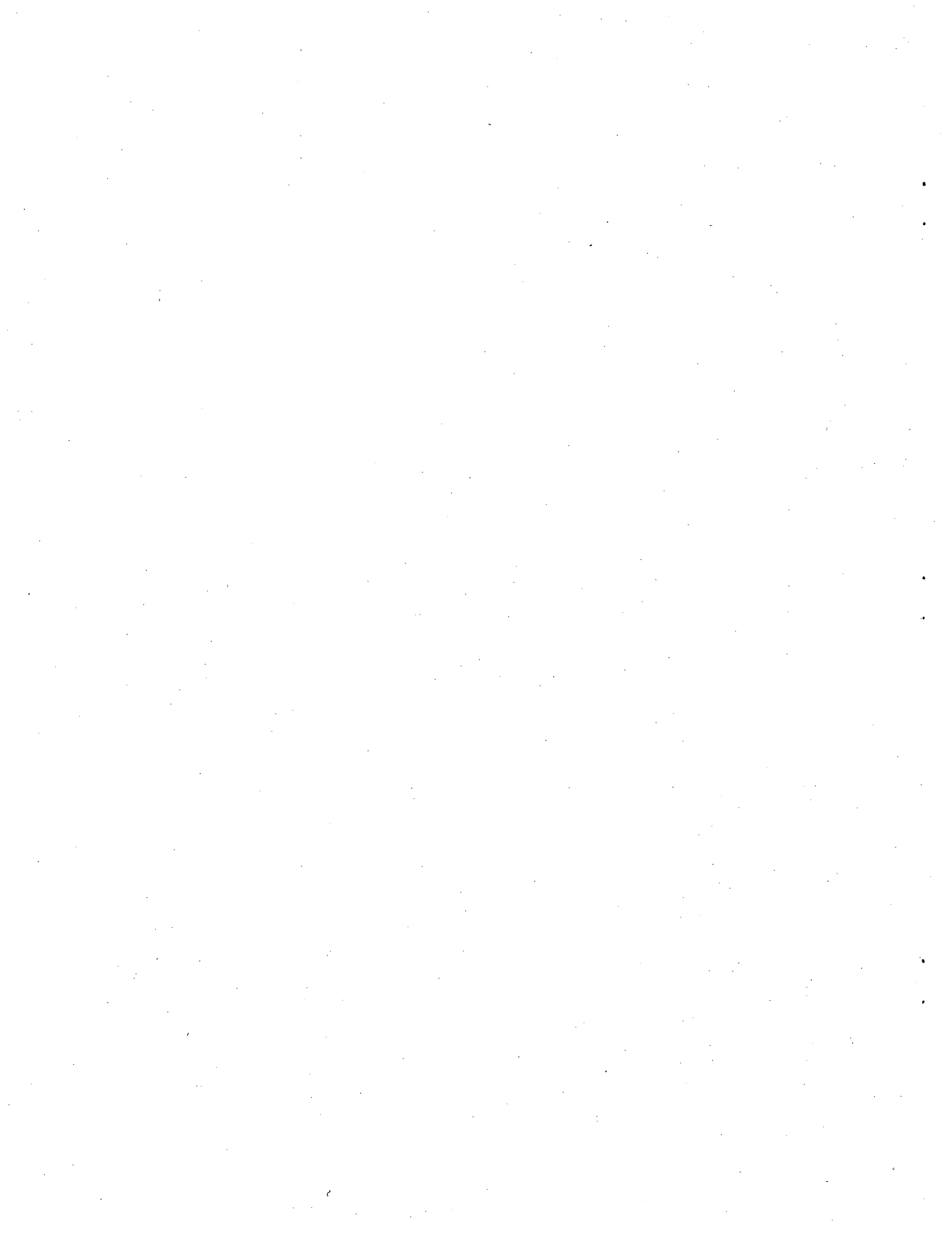


3 4456 0551783 9



CONTENTS

ABSTRACT	1
INTRODUCTION	1
CRACK GROWTH UNDER CREEP CONDITIONS	2
MATERIAL CHARACTERIZATION	3
EXPERIMENTAL PROCEDURE	4
RESULTS	7
Correlation with σ_{net} or K	7
Crack Tip Morphology	10
DISCUSSION	17
Creep Crack Growth	17
Crack initiation	17
Correlation of creep crack growth rates	18
Correlation by two parameters	21
Review of Fatigue Crack Growth Data	22
CONCLUSIONS	31
ACKNOWLEDGMENTS	31
REFERENCES	31



CRACK PROGAGATION IN HASTELLOY X

T. Weerasooriya and J. P. Strizak

ABSTRACT

The fatigue and creep crack growth rates of Hastelloy X were examined both in air and impure helium. Creep crack growth rate is higher in air than in impure helium at 650°C. Initial creep crack growth from the original sharp fatigue crack is by an intergranular mode of fracture. As the cracking accelerates at higher stress intensities, growth is by a mixed mode of both intergranular and transgranular fracture. Fatigue crack growth rate increases with increasing temperature and decreasing frequency for the range of stress intensities reported in the literature and is lower in impure helium than in air.

INTRODUCTION

In the steam cycle High-Temperature Gas-Cooled Reactor (HTGR) the fission heat generated in the reactor core is transferred by high-pressure helium coolant gas to steam generators that produce superheated steam. The primary coolant outlet temperature in the HTGR lies between 648 and 816°C. Hastelloy X is a candidate material for the outlet ducts, inlet ducts, and thermal barrier cover plates surrounding the HTGR reactor core and for ducting, tubes, or support-plate material of the intermediate and process heat exchangers^{1,2} of gas-cooled-reactor process heat plants.

Hastelloy X, a Ni-Cr-Fe-Mo alloy (nominally 47, 23, 19, and 9 wt %, respectively), has been used for more than two decades in elevated-temperature applications requiring both oxidation resistance and high strength. It is a nominal single-phase alloy with face-centered cubic structure. Strengthening is primarily by solid-solution alloying with chromium, molybdenum, and tungsten. However, carbide particles also strengthen this alloy at some temperatures.

Design against creep failure is generally based on the creep deformation and rupture data obtained in the laboratory. Stresses are

selected such that the time to initiate significant cracking exceeds the design life of the component. However, small defects may exist in the structures before they go into service or may result from creep-fatigue interaction, high-cycle fatigue, faulty machining, welding, or corrosion. In elevated-temperature design the assumption that flaws exist is changing the philosophy of design toward consideration of both initiation and propagation of cracks.

This report presents results of creep crack growth tests conducted on Hastelloy X at 650°C in both air and impure helium. We also attempt to identify the micromechanism of creep crack growth in Hastelloy X. Fatigue crack growth tests on Hastelloy X that appear in the literature are also reviewed.^{3,4}

CRACK GROWTH UNDER CREEP CONDITIONS

Several authors⁵⁻⁷ have related creep crack growth to elastic stress intensity factor by

$$da/dt = AK^n, \quad (1)$$

where

- a = crack length;
- t = time;
- K = elastic stress intensity factor;
- A and n = constants for any material, temperature, and specimen thickness.

Net section stress (σ_{net}) also has been used to correlate the creep crack growth rate.⁷⁻⁹ In addition to the above the following criteria have been used by various researchers to correlate creep crack growth rate: crack opening displacement rate ($\dot{C}OD$)⁷⁻¹⁰ and path independent rate integral (\dot{J}) or nonlinear energy release rate (C^*).¹¹⁻¹²

MATERIAL CHARACTERIZATION

Specimens for this study were fabricated from solution-annealed 12.5-mm-thick Hastelloy X plates (heat 2600-3-4936) purchased from Cabot-Stellite. Furthermore, the alloy has a grain size of 80 μm and a chemical composition as follows:

<u>Element</u>	<u>Content, wt %</u>	<u>Element</u>	<u>Content, wt %</u>
Ni	Balance	Si	0.44
Cr	21.82	C	0.07
Co	1.68	Mn	0.58
Mo	9.42	S	<0.005
Fe	19.09	W	0.63

The microstructure is shown in Fig. 1. The same material was used for the fatigue crack growth studies reported by Corwin.⁴

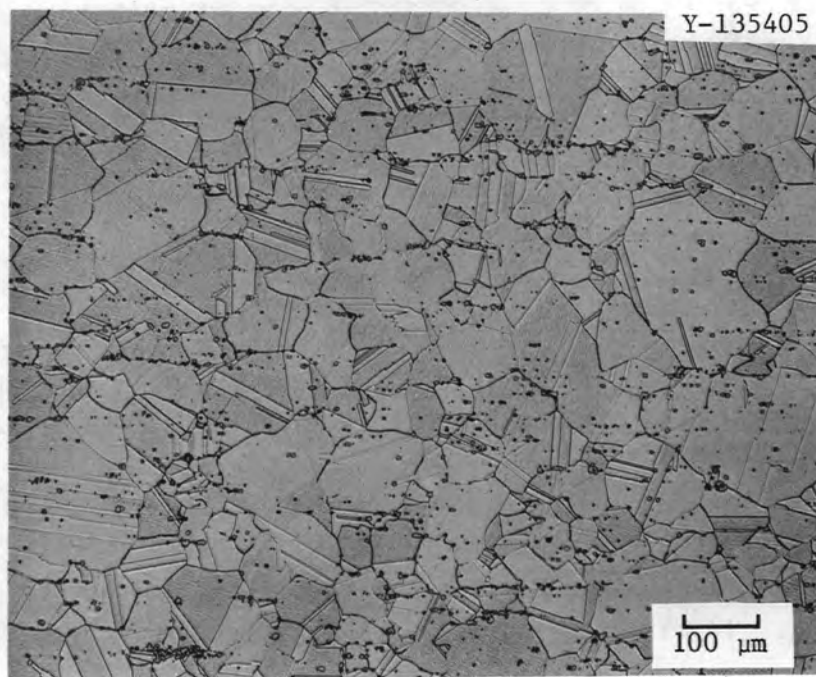


Fig. 1. Microstructure of the As-Received Hastelloy X (Heat 2600-3-4936).

An environmental chamber was used for tests that were conducted in impure helium. The composition of the impure helium was as follows:

<u>Impurity</u>	<u>Amount (wt ppm)</u>
H ₂	230-290
CH ₄	20-30
CO	10-15
H ₂ O	1-5
O ₂	<0.1

More details about the setup to supply impure helium for the test chambers are discussed elsewhere.² Figure 3 shows the test setups used for creep crack growth studies in air (right) and in impure helium (left). Details of the equipment used for fatigue crack growth work are reported by Corwin.⁴

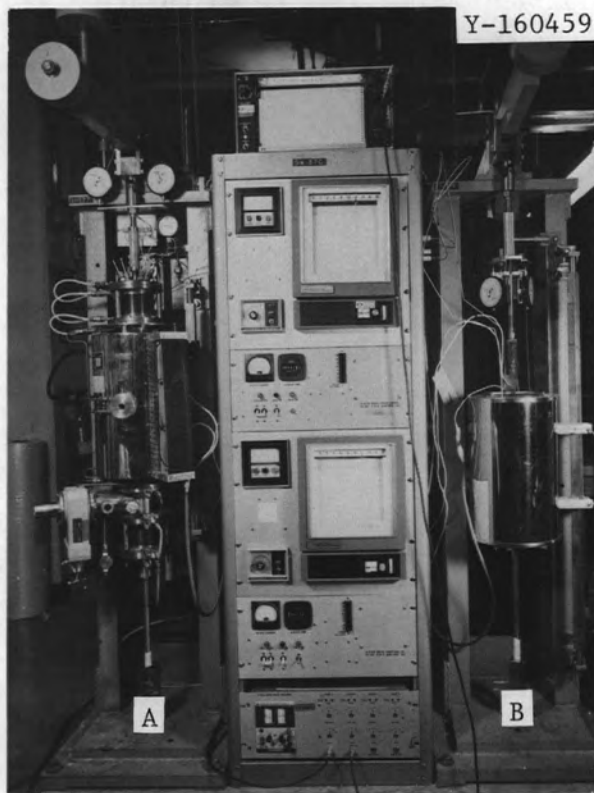


Fig. 3. Test Setups Used for Creep Crack Growth Testing.
A - impure helium chamber. B - air chamber.

Crack growth rate was computed after fitting a smooth cubic spline curve along the experimental crack length data.¹⁵ The difference between the experimental data and the data generated by the cubic spline for the crack length could be varied by S in Eq. (2):

$$\sum_{i=1}^N [a_i - a_{i(fit)}]^2 = S^2 N, \quad (2)$$

where

- a_i = measured crack length,
- $a_{i(fit)}$ = fitted crack length,
- S = 0.0025 mm and can be considered a measure of confidence in crack length readings.

The stress intensity expression used to calculate K is:

$$K = (P/B\sqrt{W}) [1.99(a/W)^{0.5} - 0.41(a/W)^{1.5} + 18.7(a/W)^{2.5} - 38.50(a/W)^{3.5} + 53.86(a/W)^{4.5}], \quad (3)$$

where

- P = load,
- B = specimen thickness,
- a = crack length,
- W = specimen width.

The expression used to calculate net section stress (σ_{net}) of the uncracked ligament is:

$$\sigma_{net} = P/[B(W - a)]. \quad (4)$$

Least square regression lines were fitted to the plots of $\log da/dt$ vs $\log K$ and $\log da/dt$ vs $\log \sigma_{net}$. The values of the constants A_1 , A_2 , n_1 , and n_2 were computed from the fitted least square regression lines for the following equations:

$$da/dt = A_1 K^{n_1}, \quad (5)$$

and

$$da/dt = A_2 \sigma_{net}^{n_2}. \quad (6)$$

RESULTS

Correlation with σ_{net} or K

As mentioned earlier other investigators have correlated creep crack growth rate with either σ_{net} or K . The creep crack propagation rates in SENT specimens are plotted as a function of elastic stress intensity (K) in Fig. 4. The elastic stress intensity was calculated by using Eq. (3). This figure shows a quite appreciable scatter of the data points and that crack growth rate of Hastelloy X in air is an order of magnitude twice the creep crack growth rate of Hastelloy X in impure helium. This higher crack growth rate in air may result from the higher oxidation at the crack tip in air. Both in air and impure helium, creep crack growth occurred by a similar micromechanism, which will be discussed later in this report.

Figure 5 gives the creep crack growth rate plotted as a function of net section stress (σ_{net}) for tests conducted both in impure helium and air.

Correlation coefficients for the lines plotted in Figs. 4 and 5 are: $K = 0.89$ and $\sigma_{net} = 0.90$ in air, and $K = 0.90$ and $\sigma_{net} = 0.92$ in impure helium.

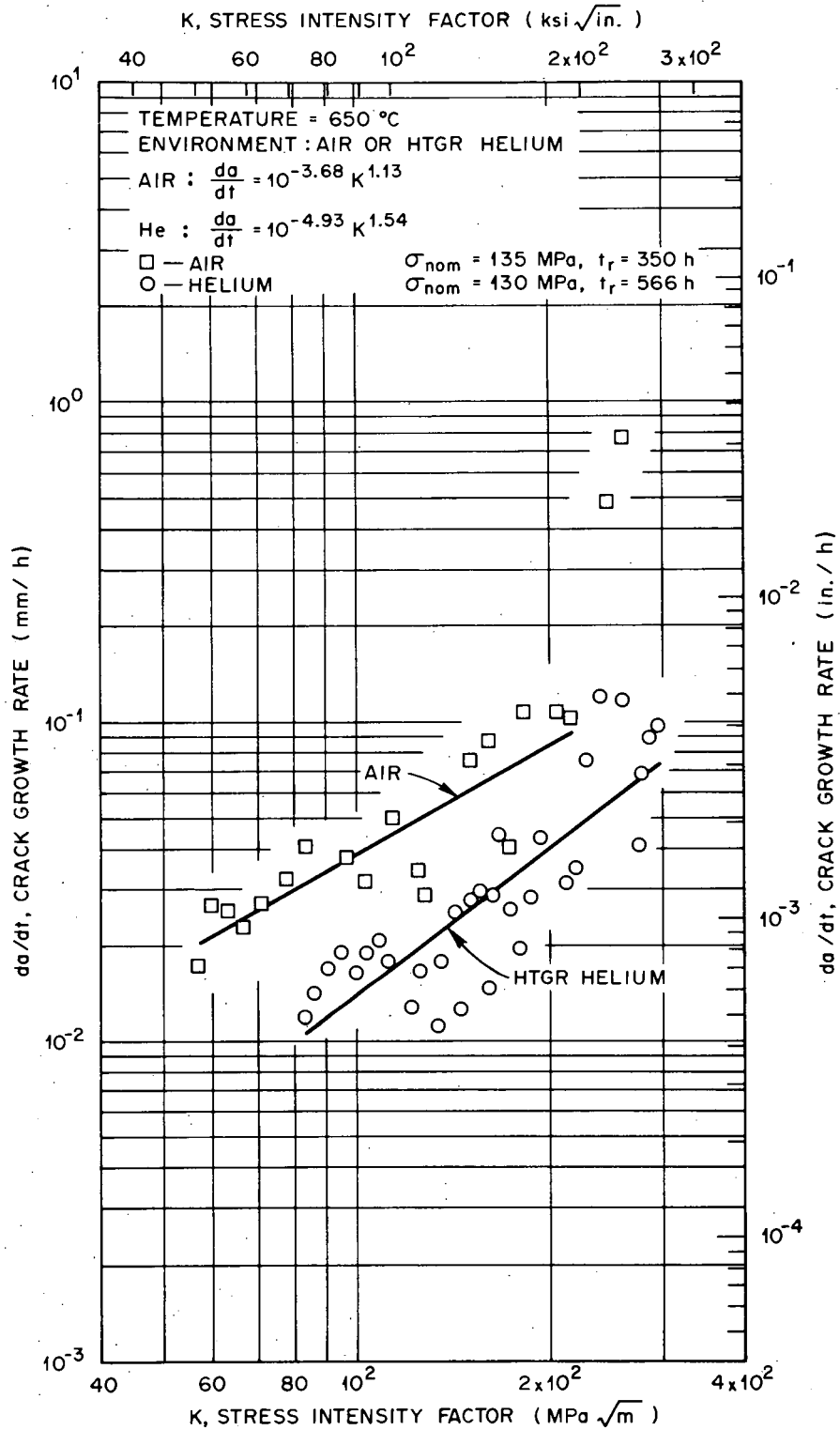


Fig. 4. The Effects of Both Air and High-Temperature Gas-Cooled Reactor Helium on the Creep Crack Growth Rate of Hastelloy X at 650°C. Creep crack growth rate (da/dt) is correlated with stress intensity (K).

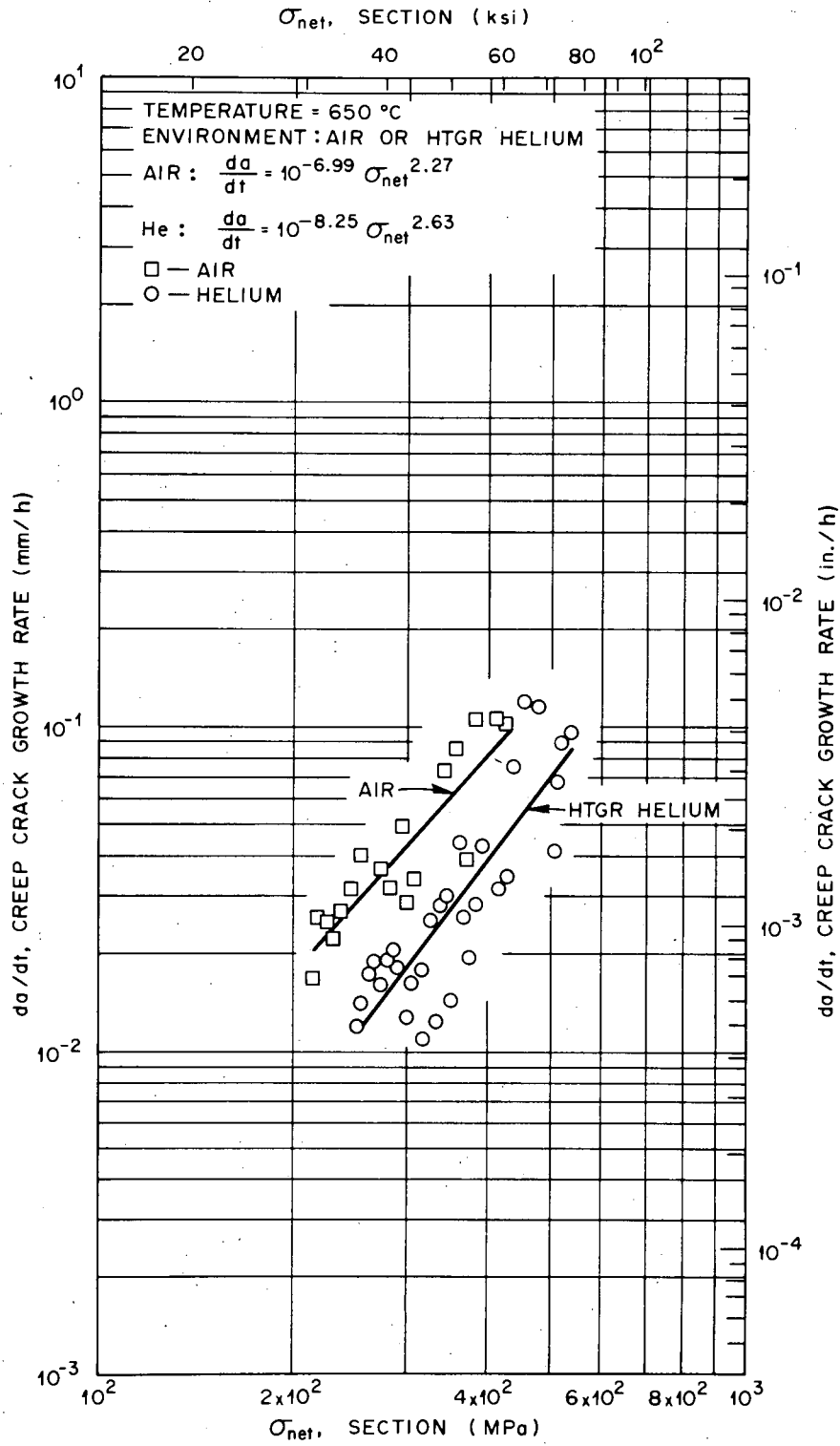


Fig. 5. The Effects of Both Air and High-Temperature Gas-Cooled Reactor Helium on the Creep Crack Growth Rate of Hastelloy X at 650°C. Creep crack growth rate (da/dt) is correlated with net section stress (σ_{net}).

Though the correlation coefficients do not differ significantly, correlation of creep crack growth rate with net section stress, σ_{net} , is slightly better than with stress intensity factor, K , for both air and impure helium.

Crack Tip Morphology

Figure 6 shows crack tip morphology as a function of time for a creep crack growth test conducted at 650°C in air ($\sigma_{nom} = 135$ MPa, $\sigma_{net} = 205$ MPa, and $K_0 = 50$ MPa m). During incubation the original fatigue crack tip opens and leads to blunting. From this blunted crack a sharp crack propagates as shown in Fig. 6(a). In initial stages of propagation of the crack the plastic deformation ahead of the crack tip is negligible. Also at this stage no appreciable amount of necking occurs at the crack tip. Figures 7 and 8 show the fracture surface at the above discussed initial stage of growth of the crack. In these photomicrographs triple point cracks that are perpendicular to the main crack front are also visible.

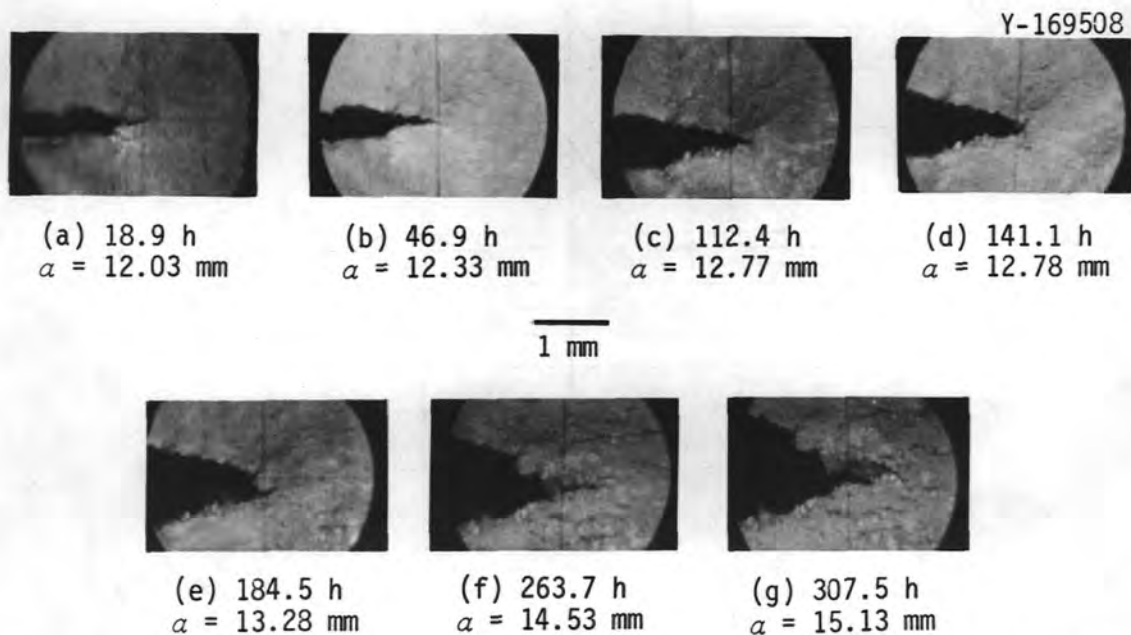
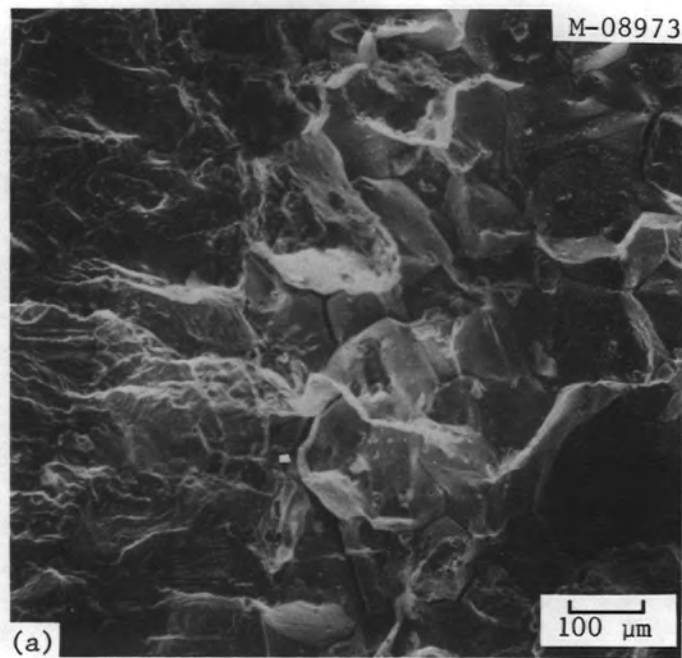
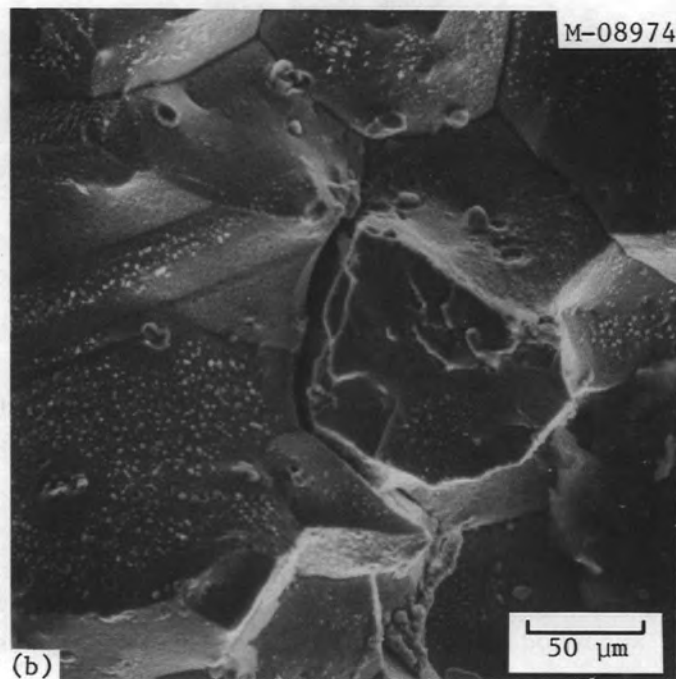


Fig. 6. Crack Tip Geometry for Hastelloy X Single-Edge Notch Tension Specimen Tested in Air at 650°C ($\sigma_{net0} = 205$ MPa, $K_0 = 50.1$ MPa m, and $a_0 = 11.73$ mm).



Direction of Propagation of Crack →



Direction of Crack Growth →

Fig. 7. Scanning Electron Micrographs of the Fracture Surface of the Creep Crack at 650°C in Air. (a) Lower left-hand corner shows the fatigued precrack. Initial propagation is intergranular. (b) At higher magnification, formation of secondary crack along the grain boundaries perpendicular to the main crack surface can be seen.

Y-160772



Direction of Crack Growth ←

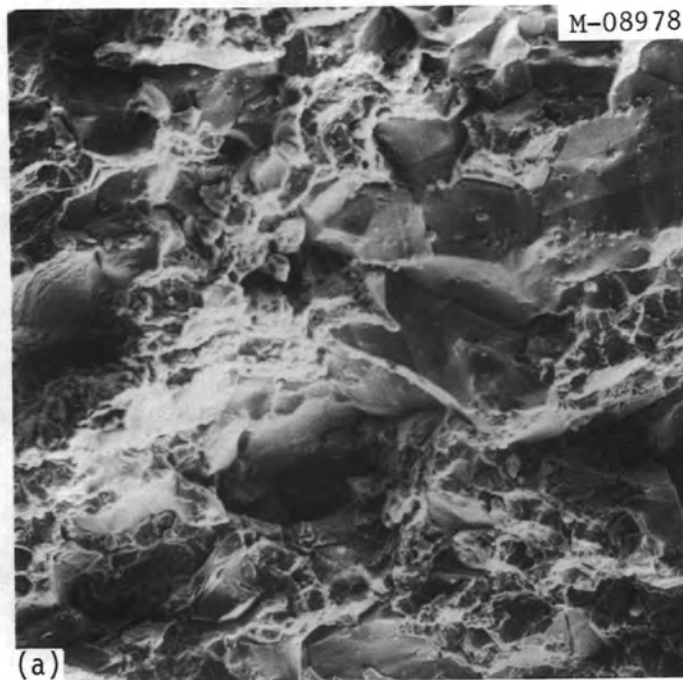
Fig. 8. The Initial Phase of Crack Growth Showing Intergranular Fracture. Secondary perpendicular intergranular and triple point cracks are also visible.

The initial stage of propagation of the crack was by an intergranular mode, and in the area ahead of the crack tip cavitation was not observed.

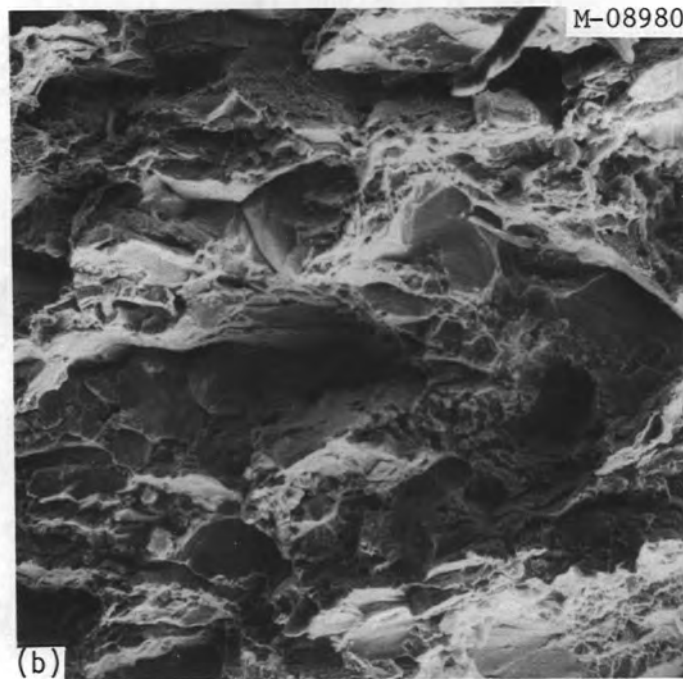
When the crack front reaches the stage shown in Fig. 6(c), deformation at the crack tip and area just ahead of the crack is easily visible. Because of the large deformations at the crack tip, blunting occurs with large accommodating crack opening displacements. Then a sharper crack initiates and propagates from this blunted tip [Fig. 6(e)]. At this stage of crack growth, cavities that have formed in the zone of intensely deformed material just ahead of the tip begin to interact with the advancing tip. This may be seen in Fig. 6(f), in which a cavity just

ahead of the crack tip has just begun to interact with the blunted tip. Thereafter, the propagation was by plastic tearing of the material between the crack tip and the cavity just ahead of the tip, as can be seen in Fig. 6(g). Cavities that have formed ahead of the tip are intergranular, and hence the propagation was that of a mixed mode of intergranular and transgranular fracture. Scanning electron fractographs in Fig. 9 show progressive changes in the fracture surface with time. In these figures grain boundary fracture facets are joined by regions of ductile tearing. As time elapses the area associated with grain boundary fracture decreases. This results from the increase of the crack driving force, that is K , σ_{net} , $C\dot{O}D$, or \dot{J} , which changes the fracture mechanism from an intercrystalline fracture to a transgranular one. The grains are deformed (Fig. 10), indicating that a great deal of shear strain took place before fracture. A certain amount of grain boundary sliding may have also occurred. Figure 11 shows the fracture surface close to the surface of the specimen at the later stages of the growth of the crack. Although the fracture is mixed, with both intergranular as well as ductile transgranular regions, the grains are deformed and elongated in the direction of the nominal stress (σ_{nom}), indicating that ductile, transgranular fracture was the predominant mode of failure.

Figure 12 shows the magnified view of both sides of the crack tip at the same instant shown in Fig. 6(g). Cracks ahead of the main tip are zigzag, inclined 45° to the direction of the uniaxial stress. Figure 12(b) clearly shows the propagation of the blunted main crack by joining with small cracks ahead of the main tip. Figure 13 shows the last stages of crack growth. Though the crack has propagated mainly by a transgranular mode, cavities have formed along the grain boundaries, indicating that the cracks formed ahead of the crack tip are intergranular. Figure 14 shows the morphology of the blunted fatigue crack tip, which did not propagate even after 1680 h. The crack tip shows a considerable amount of plastic deformation. Cavities forming ahead of the tip are also visible.



100 μm



Direction of Crack Growth →

Fig. 9. Scanning Electron Micrographs of Fracture Surface. (a) Large areas of grain boundary fracture joined by ductile mode of fracture. (b) Last stages of crack growth. Few areas of undeformed grain boundaries are present. Fracture is mainly a ductile mode.



Direction of Crack Growth ←

Fig. 10. Intergranular Cavities are Joined by Transgranularly Deformed Regions. Grain surfaces are also deformed.

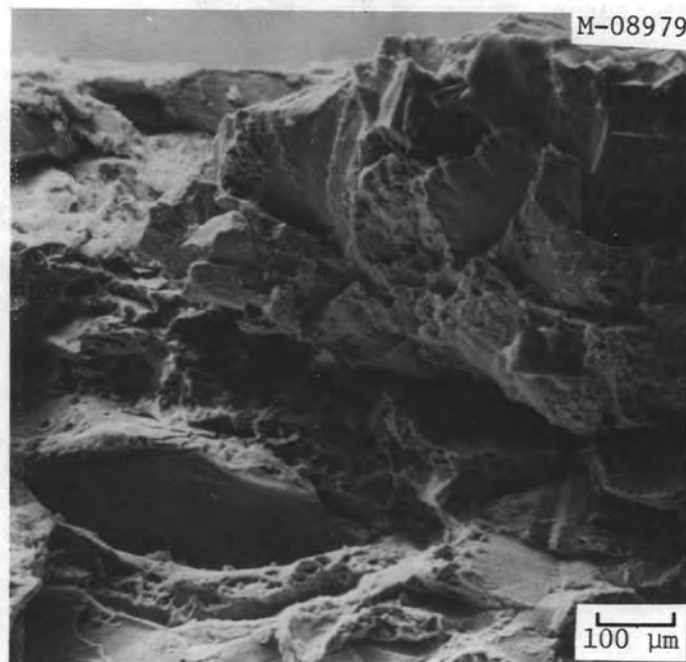


Fig. 11. Fracture Surface Close to the Surface of the Specimen.

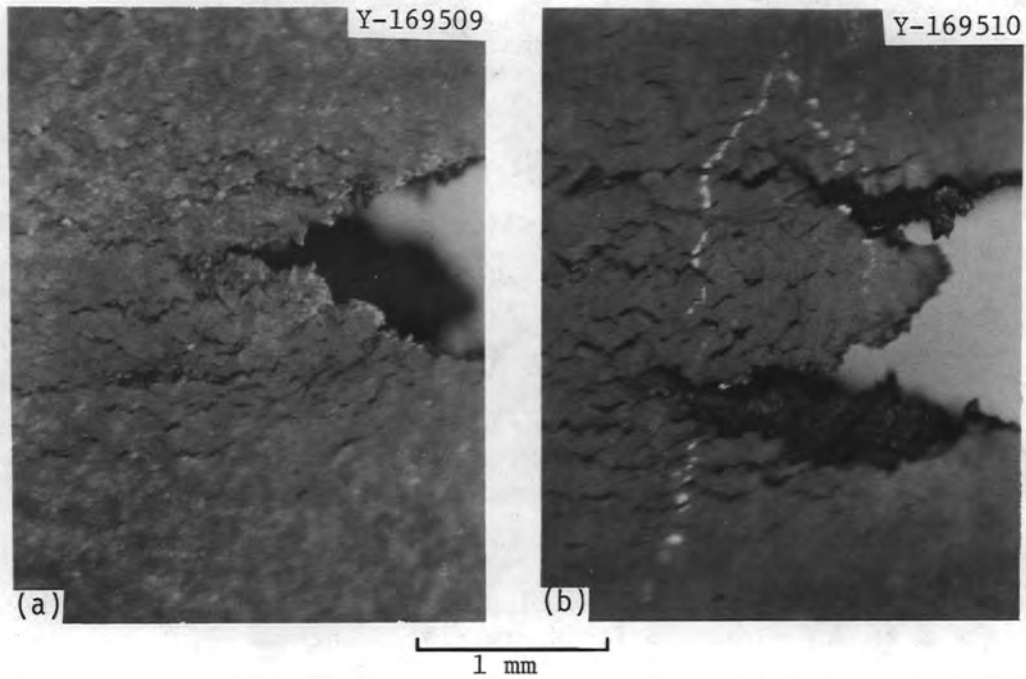


Fig. 12. Morphology at Both Sides of the Crack Tip after 307.5 h. This is the same instant shown in Fig. 6(g).

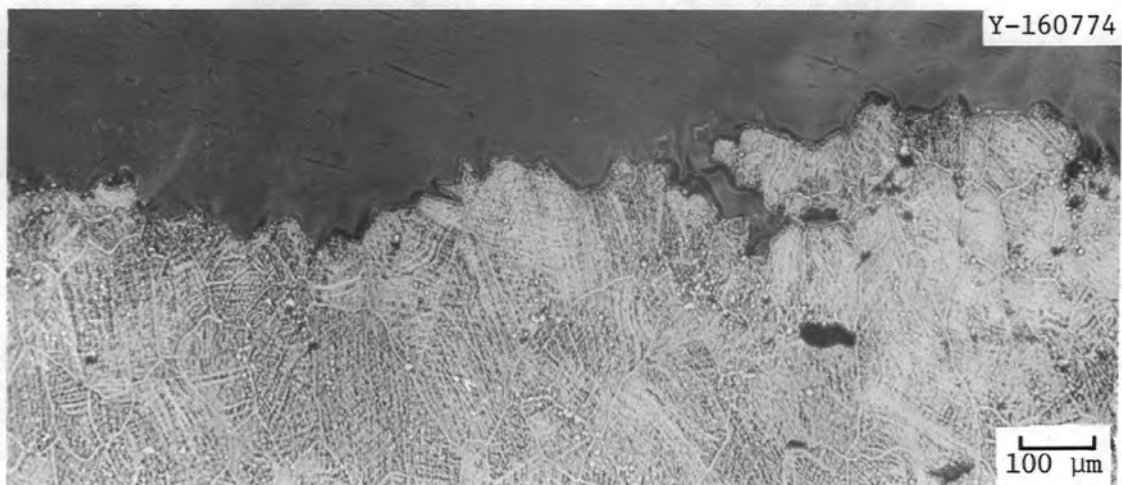


Fig. 13. Last Stages of Crack Growth. Crack propagated mainly by a ductile mode, but deformed grain boundary cavities are present.

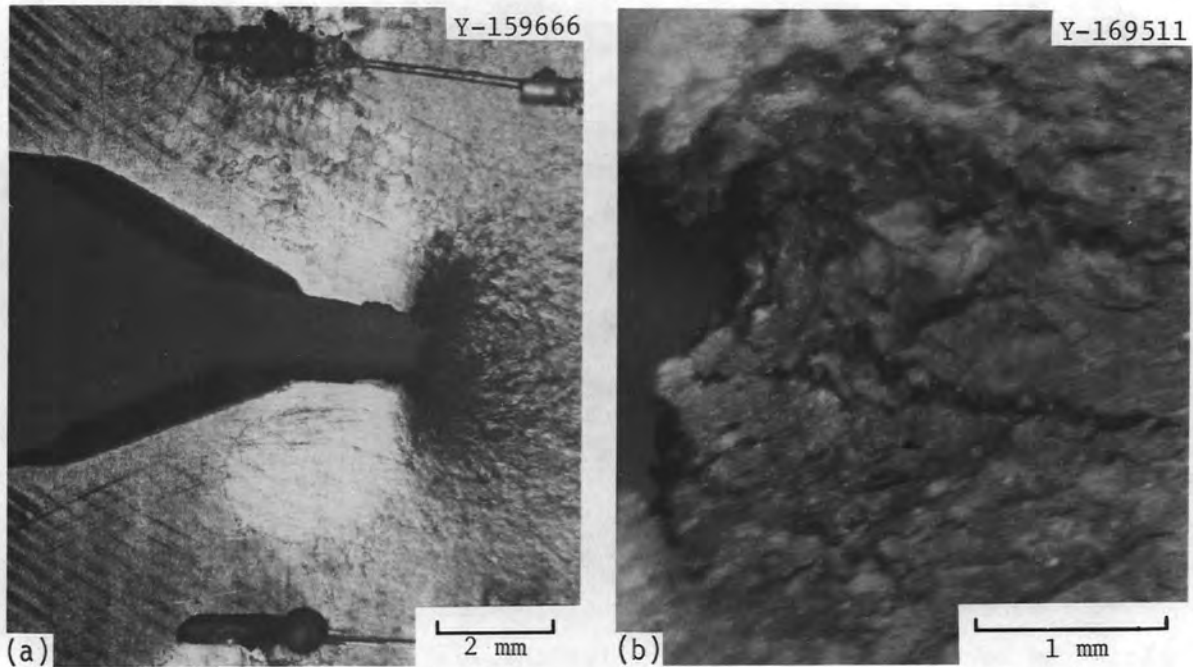


Fig. 14. Morphology of the Crack Tip After 1680 h. (a) The crack tip blunted and did not propagate ($\sigma_{nom} = 88$ MPa). (b) Magnified view at the crack tip.

DISCUSSION

Creep Crack Growth

Crack initiation

In our creep crack growth tests the mode of crack initiation was intergranular. The initial sharp fatigue crack had an influence on the mechanism of initiation of the creep crack because the initial "quasi-brittle" behavior results from constraint. Increasing the initial crack tip radius would have reduced the observed "brittleness" at the beginning by the reduction of the initial stress elevation, letting damage, that is voidage, accumulate more slowly at the tip. In this case relaxation of the intensified stress at the crack tip will be faster, leading to enhanced ductility at the tip. So the initiation process will highly depend on the process of relaxation of the stress at the tip, which in turn will depend on the constraint at the tip.

The behavior of a notched creep specimen under load will depend on two competing processes: stress intensification at the crack tip leading to growth of the crack and creep deformation at the crack tip leading to relaxation of the intensified stress. That the crack velocity is high indicates that the intensification of the stress at the tip will cause cracking before the stress can relax there. The specimen shown in Fig. 6 is a typical example of this case. The other extreme of behavior will occur when the stress relaxation at the crack tip reduces the stress intensification significantly or removes it altogether. In this case creep deformation will occur across the uncracked ligament of the specimen. When the loading is in the intermediate range, creep deformation will occur in the vicinity of the tip, and the relaxation will reduce the stress such that the tip will blunt before crack growth. This can be seen in Fig. 14, in which the loading was so low that the crack would not grow, even after 1680 h. A region of extensive plasticity, visible in the area close to the crack tip, is responsible for the stress relaxation and redistribution.

Correlation of creep crack growth rates

As discussed earlier the attempts to correlate the creep crack growth rates with K or σ_{net} ended with about the same results. In this case the stress intensity factor would have been the more logical parameter with which to correlate the creep crack growth, but still in this region while the crack was propagating, relaxation of the stresses was occurring. If the stresses had relaxed completely (Fig. 15), the creep damage would occur on the whole uncracked ligament of the specimen. In this case the obvious choice for the load correlating parameter of creep crack growth would be the net section stress (σ_{net}). In the range of loading used in the present experiments, neither of the above mentioned extremes were attained. Although the initial stages of creep crack growth showed little ductility, later stages of growth resulted from creep deformation and the formation of cavities in the immediate vicinity of the crack tip. Formation of cavities ahead of the tip can be explained by referring to the relaxed stress distribution.¹⁶ The

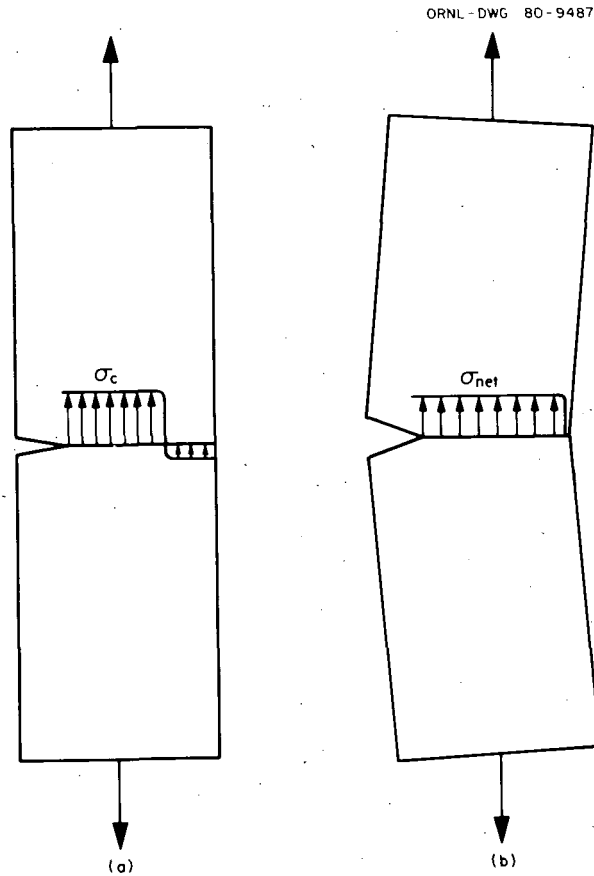


Fig. 15. Stress Distribution in Single-Edge Notch Tension specimen. (a) Normal loading. (b) Eccentric loading.

relaxing stress distribution will have its maximum value not at the crack tip, but at a distance ahead of it. The distance where the maximum stress occurs will increase with time for a stationary crack.

After the initial low-ductility crack growth, the crack grew intermittently by the ductile rupture of the material between the crack tip and the nearest cavity ahead of the tip. This intermittent growth would have also contributed to the scatter in the crack growth rate data given in this report.

Figure 15 shows the two possible configurations of the completely relaxed stress distribution of the specimen. Since the tested specimens were loaded with a pin (Fig. 16) the specimen is allowed to rotate so that the bending component of the stress on the uncracked ligament would disappear [Fig. 15(b)]. Whether this type SENT specimen would rotate

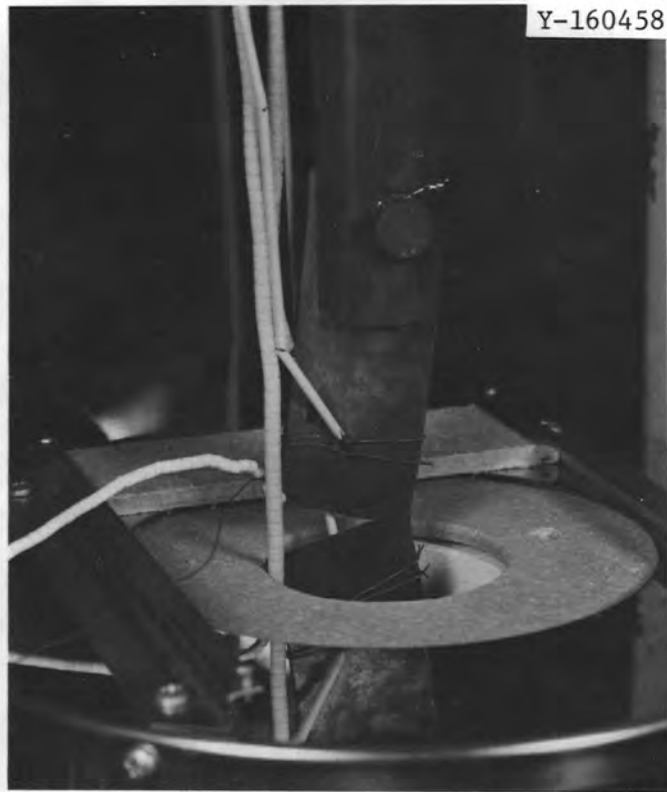


Fig. 16. Single-Edge Notch Tension Specimen That Was Tested in Air. Specimen has deformed to relieve the component of stress from bending.

enough for complete disappearance of the bending component of the stress is uncertain. This uncertainty may have also contributed to the scatter of the crack growth results when correlated with σ_{net} .¹⁷ Ideally, the center cracked panel is more suitable for studying the creep crack growth since the uncertainty from the amount of bending is not present in this type of specimen relaxation vs stress intensification.

As outlined above, initiation of a creep crack from a notch or a sharp crack and the propagation of the creep crack is governed by two competing processes: stress intensification at the crack tip and relaxation of the intensified stress at the tip. If the process of relaxation of the tip stress is slow, then the elastic strain fields dominate everywhere, except in the very small creep zone at the tip. Fracture will occur with minimum creep and plastic deformation, and the damage is confined to the crack tip. In this case the stress intensity factor should be the correlating parameter.

When the relaxation of stresses at the crack tip occurs quickly so that the zone of creep deformation is large and engulfs the whole uncracked ligament, creep deformation will occur in the whole remaining ligament. In this case stresses will become time independent, and one could speculate that the net section stress would correlate best with the creep crack growth rate. If a bending component of stress exists, then the net section stress has to be replaced by a reference stress that is equal to the relaxed tensile stress [σ_c in Fig. 15(a)].

The intermediate stage of relaxation of the crack tip stress, where the zone of creep deformation ("creep zone") is large but not large enough to engulf the remaining ligament, is identical to the large scale yielding in the fracture of monotonically loaded specimens where limit loads have not been reached. In this case one could speculate that the loading parameter that determined the near tip fields uniquely is C^* or \dot{J} .^{11,12} The C^* parameter is defined extensively in ref. 12.

When many cavities are present in the creep zone, as seen in Fig. 6, characterization of the near-tip stress and strain rate fields by the single parameter C^* is violated since a material undergoing copious cavitation is no longer governed by a steady-state creep law appropriate for a nonlinear viscous solid. Even in the absence of cavities, propagation of the crack would not allow the material adjacent to the crack tip to reach steady-state creep, that is, the strain rate would be time dependent.

Correlation by two parameters

One school of thought believes that the ductile initiation of a crack and the proceeding stable crack growth thereafter can be predicted by two parameters. At the initiation, critical value for \dot{J} or COD (path independent integral and crack opening displacement, respectively), and the stable propagation is controlled by a critical crack tip opening angle (CTOA) or a critical generalized energy release rate at the crack tip process zone.¹⁸

Similarly, the initiation and growth of a creep crack may be correlated by two parameters. Correlation will be further complicated by the interaction of the relaxation rate of the stress at the crack tip with the initiation and propagation of the creep crack.

Review of Fatigue Crack Growth Data

Figures 17 through 22 give the results of fatigue crack growth tests conducted by Corwin⁴ to find the effect of frequency, temperature, stress intensity (ΔK), and environment on the fatigue crack growth rate (FCGR) of Hastelloy X. All these tests were conducted with SENT specimens. The FCGR was correlated with ΔK by using the expression given below for a constant frequency and constant temperature:

$$da/dN = A_3 \Delta K^{n_3} \quad (7)$$

Figures 17 through 22 also give the values of A_3 and n_3 in Eq. (7), where da/dN is in mm/cycle, and ΔK is in MPa m. Figures 17 and 18 show the effect of temperature on the FCGR of Hastelloy X at frequencies 0.1 and 1.0 Hz in air. The FCGR at 871°C is about 10 times the FCGR observed at 538°C in air for both frequencies 0.1 and 1.0 Hz. The same behavior is observed in the tests conducted in impure helium (Fig. 19). As observed for creep crack growth rates, the FCGR is higher in air than in HTGR helium at 538°C (Fig. 20). This increase may possibly result from the transient creep interaction, as at 538°C, where not much oxidation occurs at the crack tip. Figure 21 gives the effect of both air and helium on the FCGR of Hastelloy X at 871°C and a frequency of 1.0 Hz. The difference in the FCGR in air and in helium is greater at 871°C compared with that at 538°C. At 871°C more transient creep and oxidation interaction at the crack tip are probably the reasons for the above observation. Figures 22 and 23 give the effect of frequency (between 0.1 and 1 Hz) on the FCGR, which is substantially smaller at both temperatures.

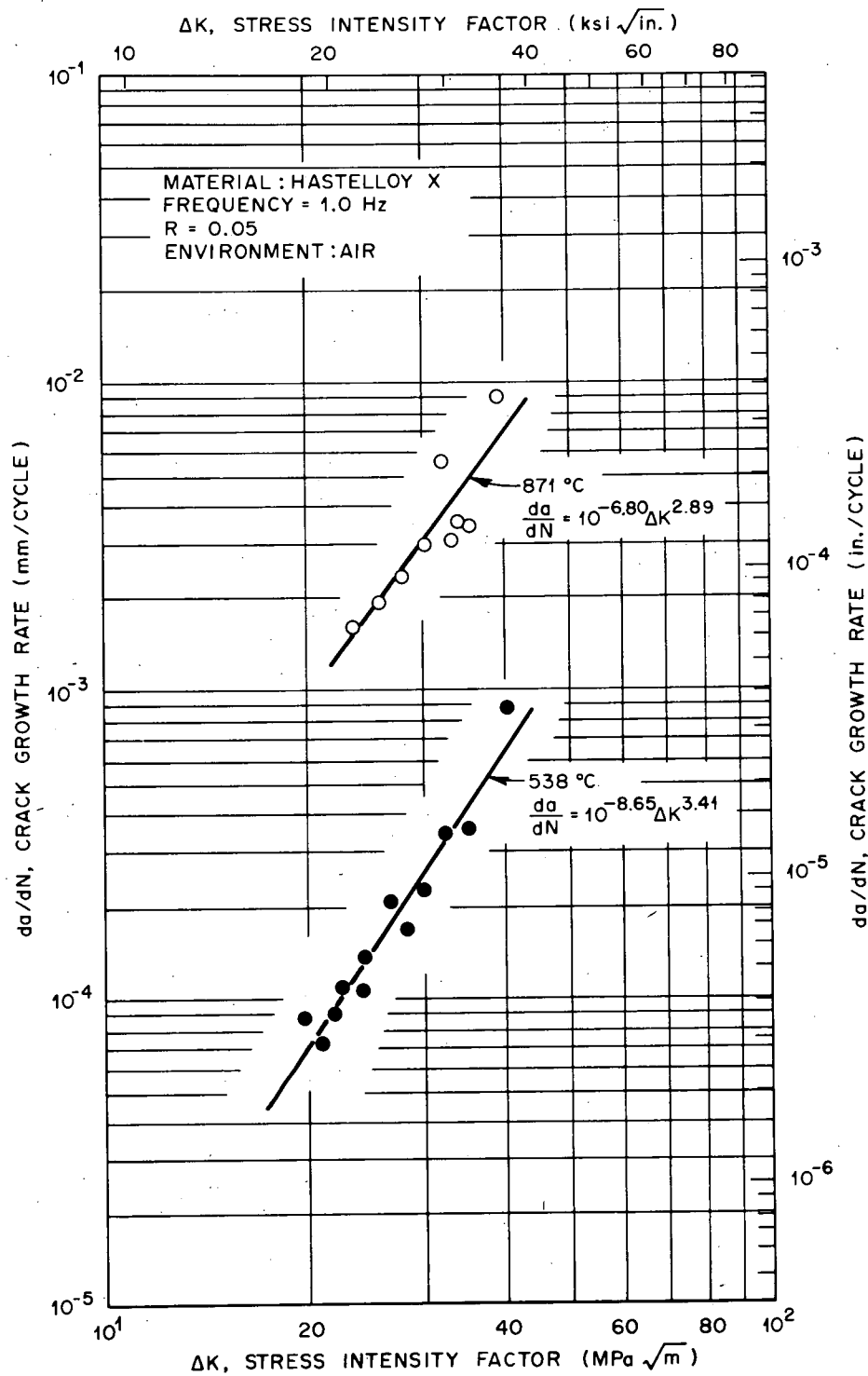


Fig. 17. The Effect of Temperature on the Fatigue Crack Growth Rate of Hastelloy X at 1.0 Hz in Air.

ORNL-DWG 79-10774

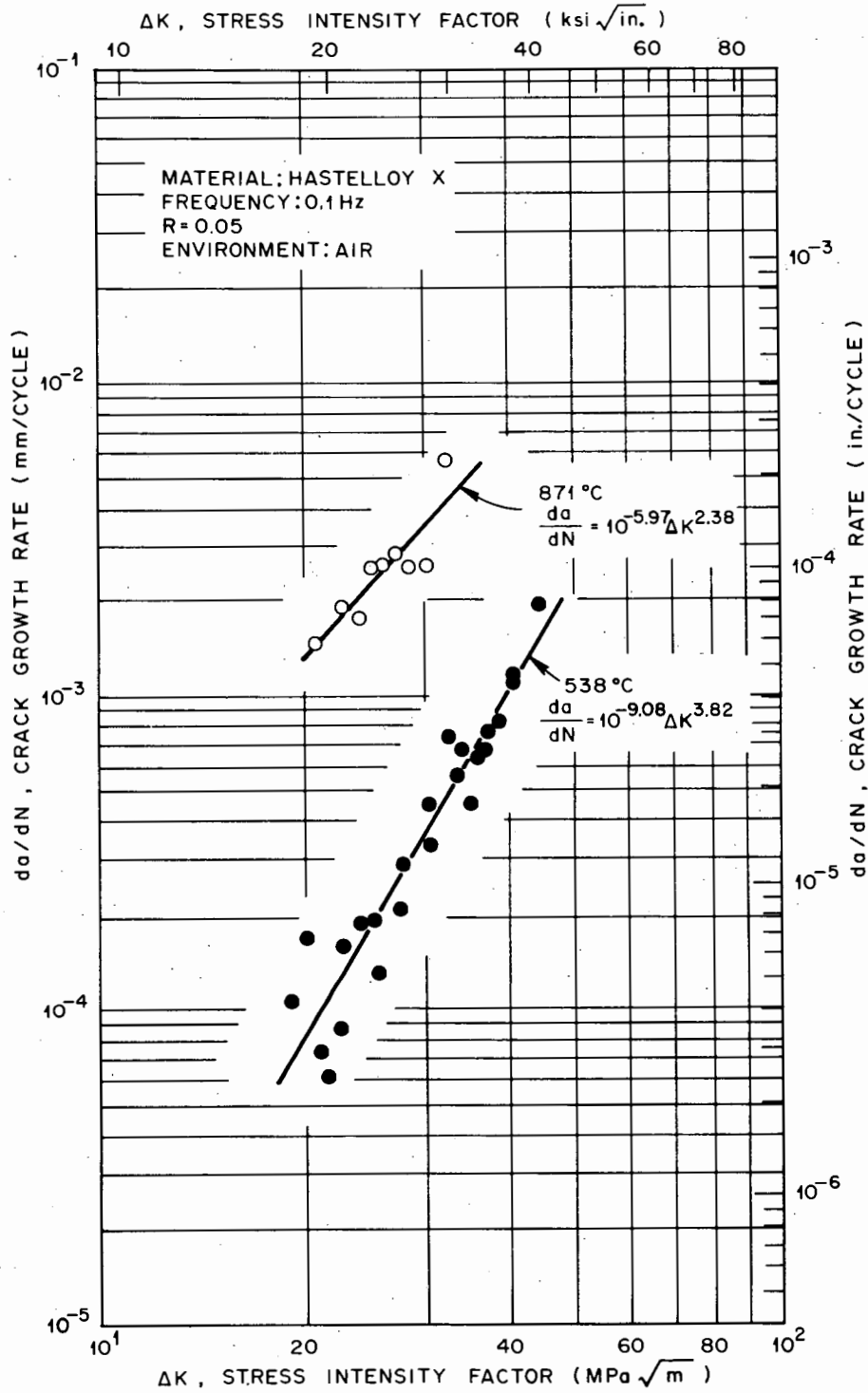


Fig. 18. The Effect of Temperature on the Fatigue Crack Growth Rate of Hastelloy X at 0.1 Hz in Air.

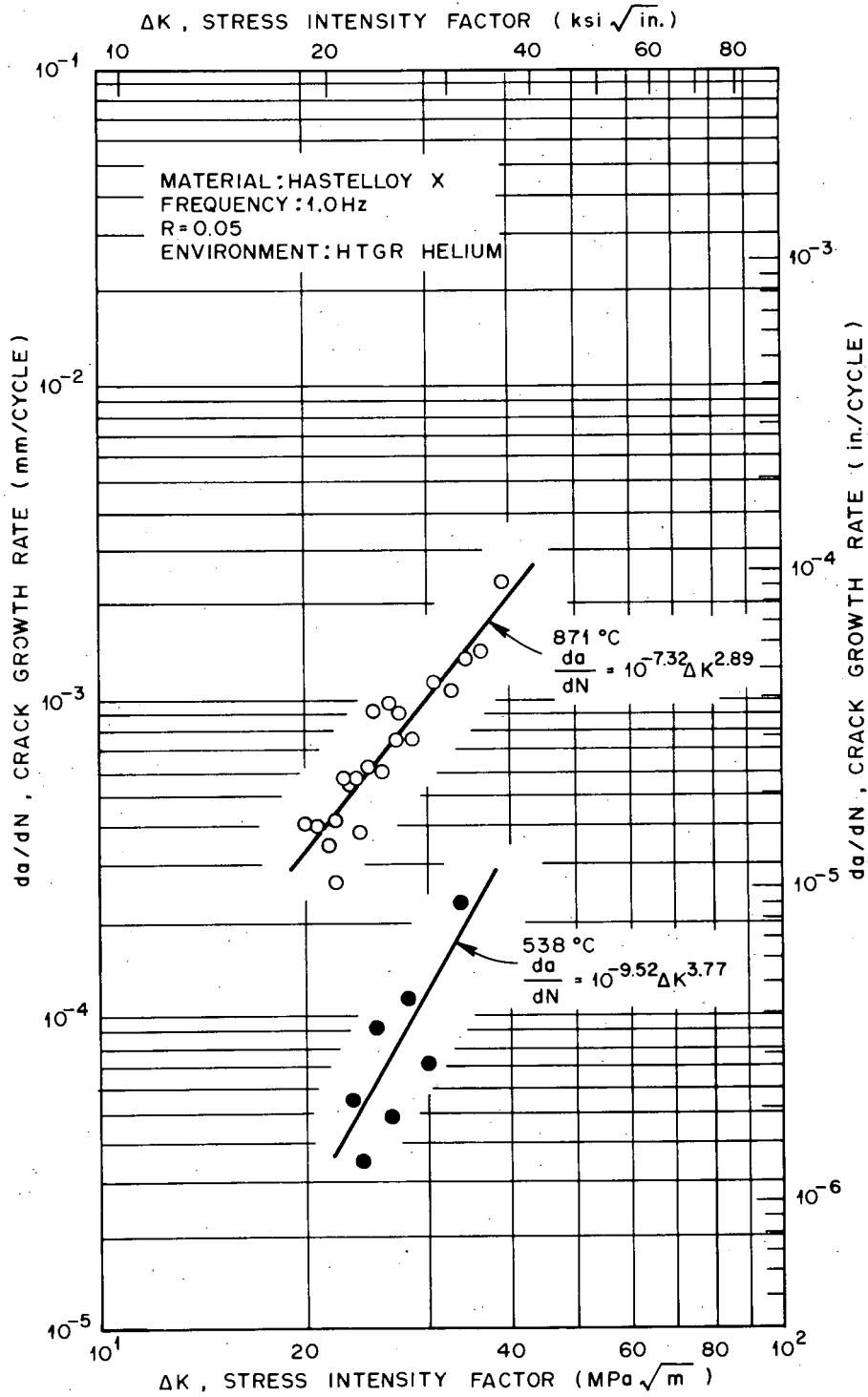


Fig. 19. The Effect of Temperature on the Fatigue Crack Growth Rate of Hastelloy X at 1.0 Hz in High-Temperature Gas-Cooled Reactor Helium.

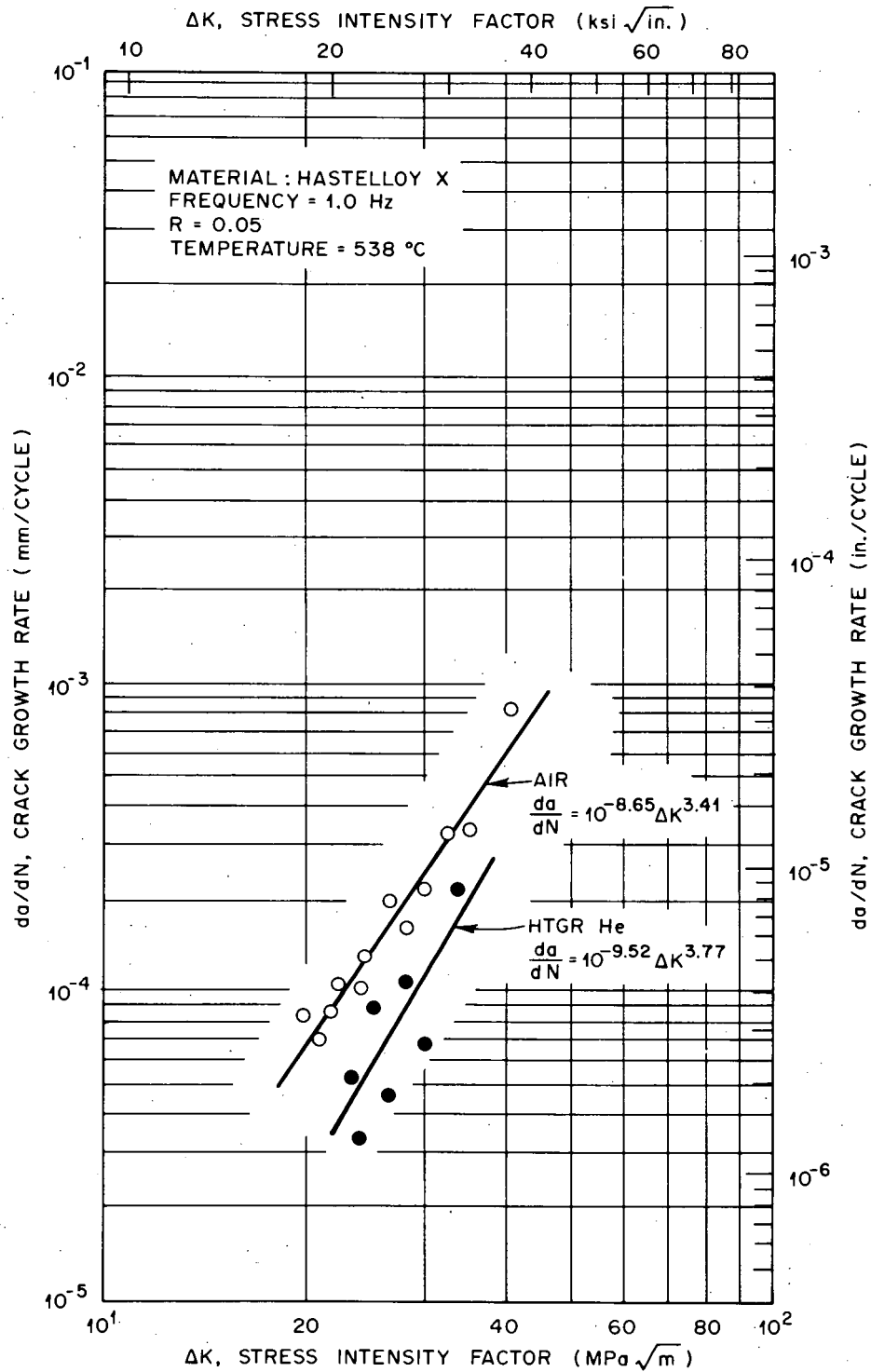


Fig. 20. The Effect of Environment on the Fatigue Crack Growth Rate of Hastelloy X at 538°C and 1.0 Hz.

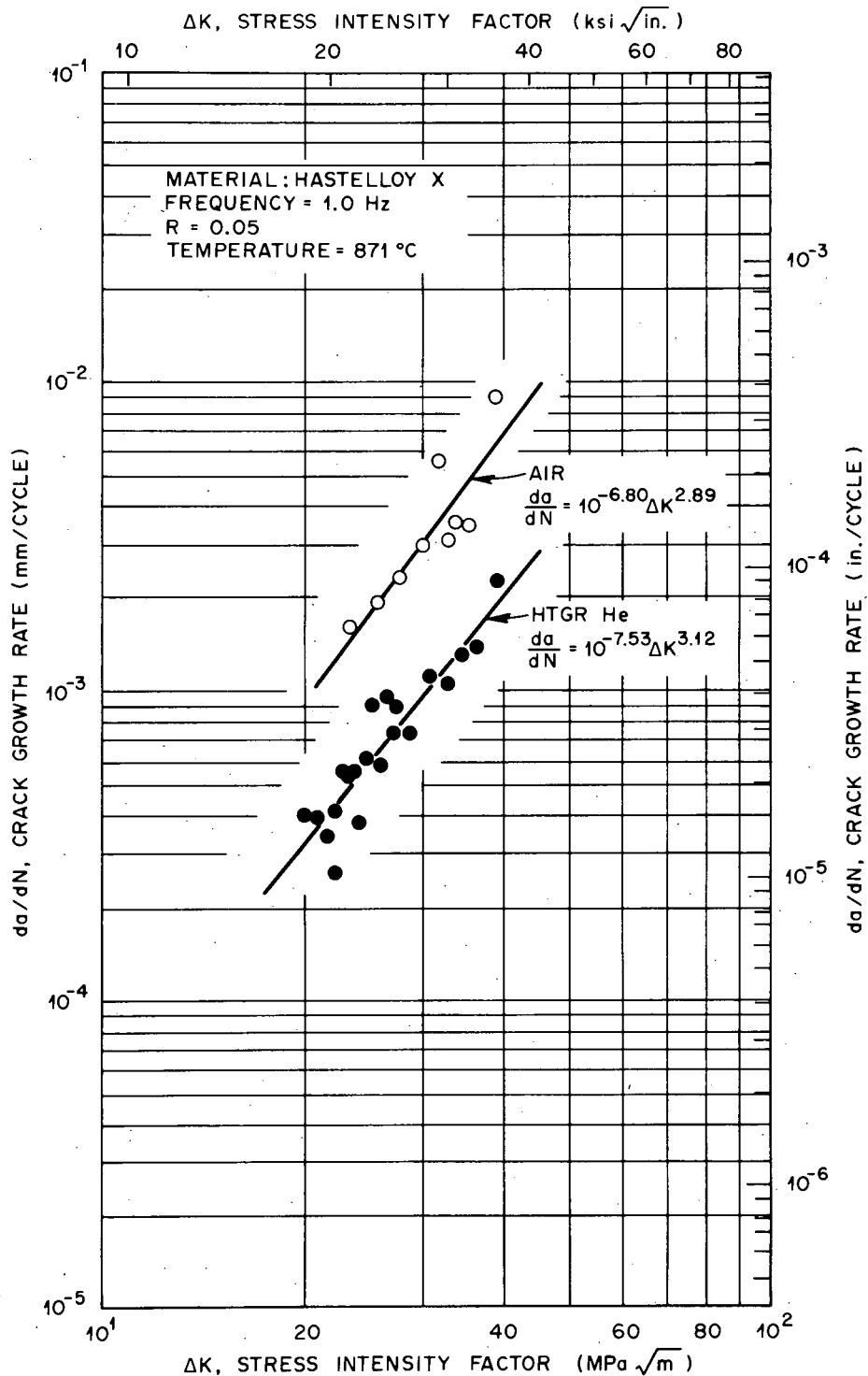


Fig. 21. The Effect of Both Air and High-Temperature Gas-Cooled Reactor Helium on the Fatigue Crack Growth Rate of Hastelloy X at 871°C and 1.0 Hz.

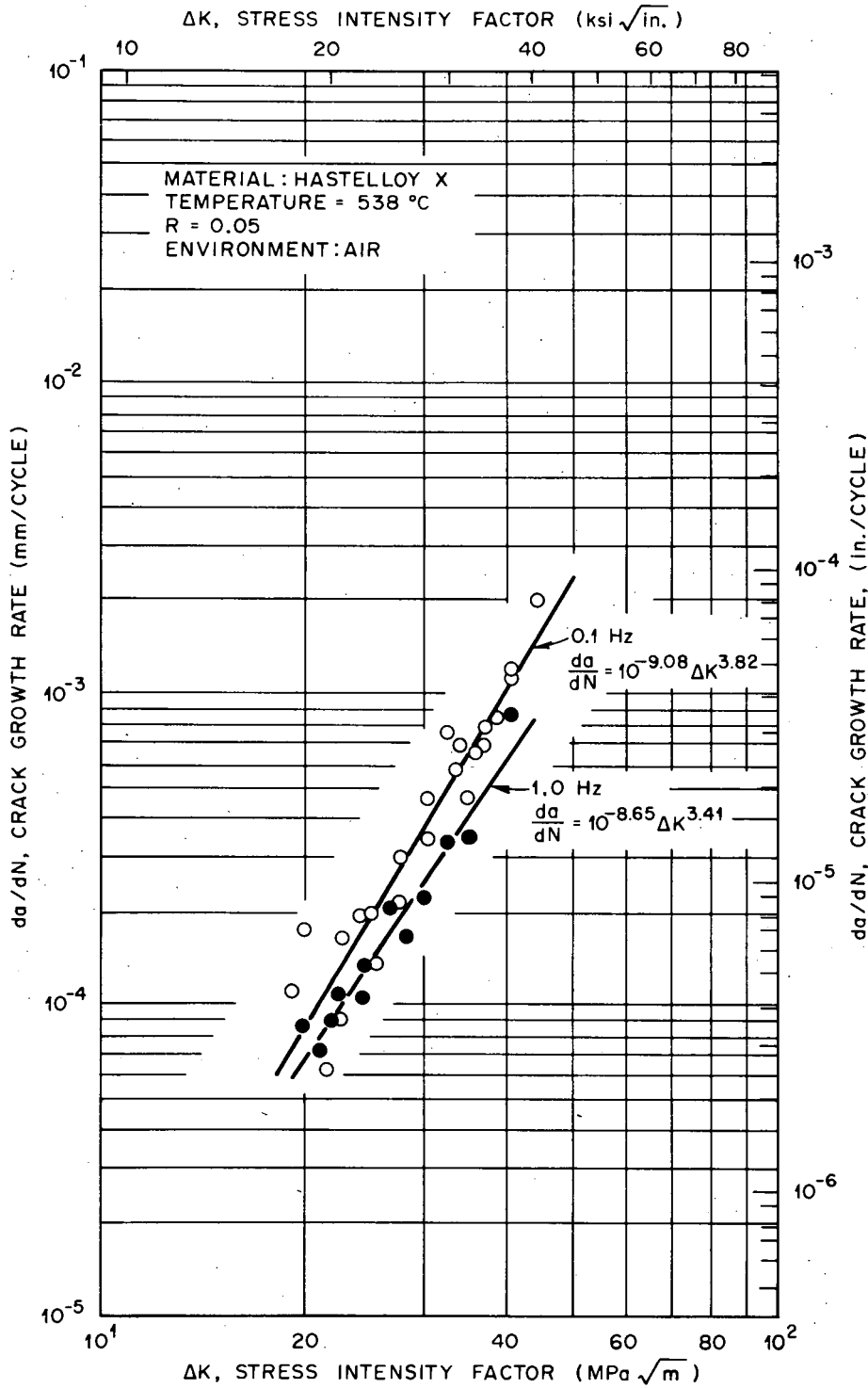


Fig. 22. The Effect of Frequency on the Fatigue Crack Growth Rate of Hastelloy X at 538°C in Air.

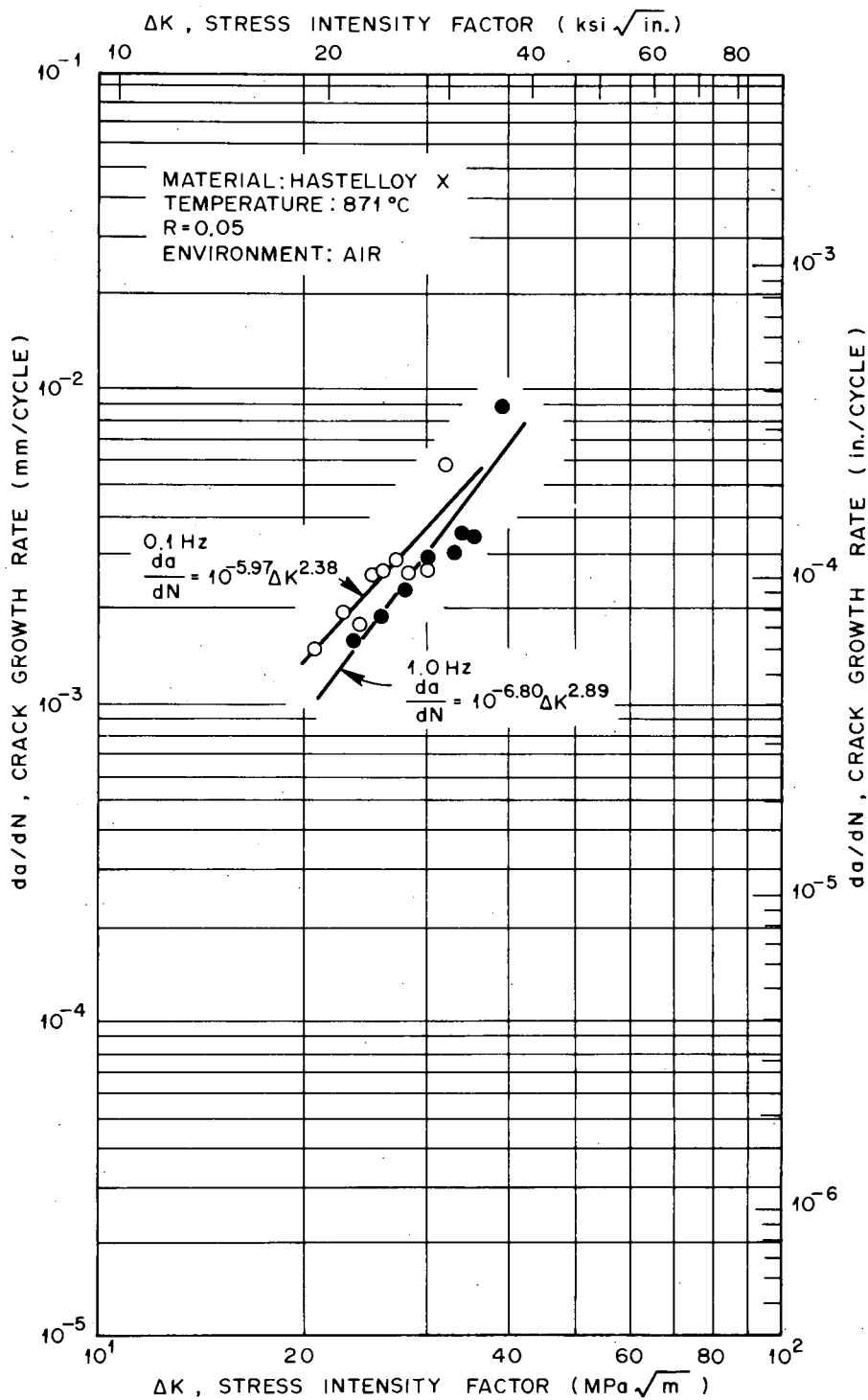


Fig. 23. The Effect of Frequency on the Fatigue Crack Growth Rate of Hastelloy X at 871°C in Air.

The FCGR also decreases with increasing frequency in vacuum.³ Hence, it can be expected that the FCGR decreases with increasing frequency in impure helium. This frequency dependence in vacuum results from the creep and strain rate dependent deformation. The tests conducted in oxygen³ at different pressures at 760°C lead to the belief that environmental interaction occurs in the tests conducted in air. Hence, the frequency dependence in air results from a combination of environmental interaction and creep and strain rate dependent deformation. Table 1 gives an estimation made by Jablonski³ on the magnitudes of these three interactions at 760°C.

Table 1. Relative Importance of Creep-Fatigue Interactions, Oxidation-Fatigue Interactions, and Strain Rate Dependent Plasticity on Hastelloy X at 760°C^a

Interaction	Magnitude (%)
<u>In Vacuum</u>	
Oxidation-fatigue	0
Creep-fatigue	67
Strain rate dependent plasticity	33
<u>In Air</u>	
Oxidation-fatigue	50
Creep-fatigue	33
Strain rate dependent plasticity	16

^aSource: D. A. Jablonski, *Fatigue Behavior of Hastelloy X at Elevated Temperatures in Air, Vacuum, and Oxygen Environments*, Ph.D. Thesis, Massachusetts Institute of Technology, Boston, January 1978.

The fracture mode of Hastelloy X changes from intergranular to transgranular by a change in frequency from 0.1 to 10 Hz.³ This was observed both in high vacuum and vacuum with oxygen [partial pressure of oxygen 1.3×10^{-3} Pa (1×10^{-5} torr)]. Vacuum promotes

more intergranular fracture compared with air at 0.1 Hz. The intergranular fracture was more pronounced for higher ΔK values.

CONCLUSIONS

1. Creep crack growth rate in air is higher than in impure helium for $800 \text{ MPa}\sqrt{\text{m}} < K < 200 \text{ MPa}\sqrt{\text{m}}$ at 650°C .
2. Two modes of creep crack growth, intergranular mode and a mixed mode of both intergranular and transgranular, were observed at 650°C .
3. The FCGR increases with increasing temperature at both 1.0 and 0.1 Hz in air and in impure helium for $20 \text{ MPa}\sqrt{\text{m}}$.
4. The FCGR is higher in air than in impure helium both at 538 and 871°C for a frequency of 1.0 Hz for $20 \text{ MPa}\sqrt{\text{m}} < \Delta K < 40 \text{ MPa}\sqrt{\text{m}}$.
5. Change in frequency from 1.0 to 0.1 Hz slightly increases the FCGR at 538 and 871°C in air for $20 \text{ MPa}\sqrt{\text{m}} < \Delta K < 40 \text{ MPa}\sqrt{\text{m}}$.
6. The mode of the FCGR changes from intergranular to transgranular as a result of change in frequency from 0.1 to 10 Hz at 760°C both in air and vacuum.

ACKNOWLEDGMENTS

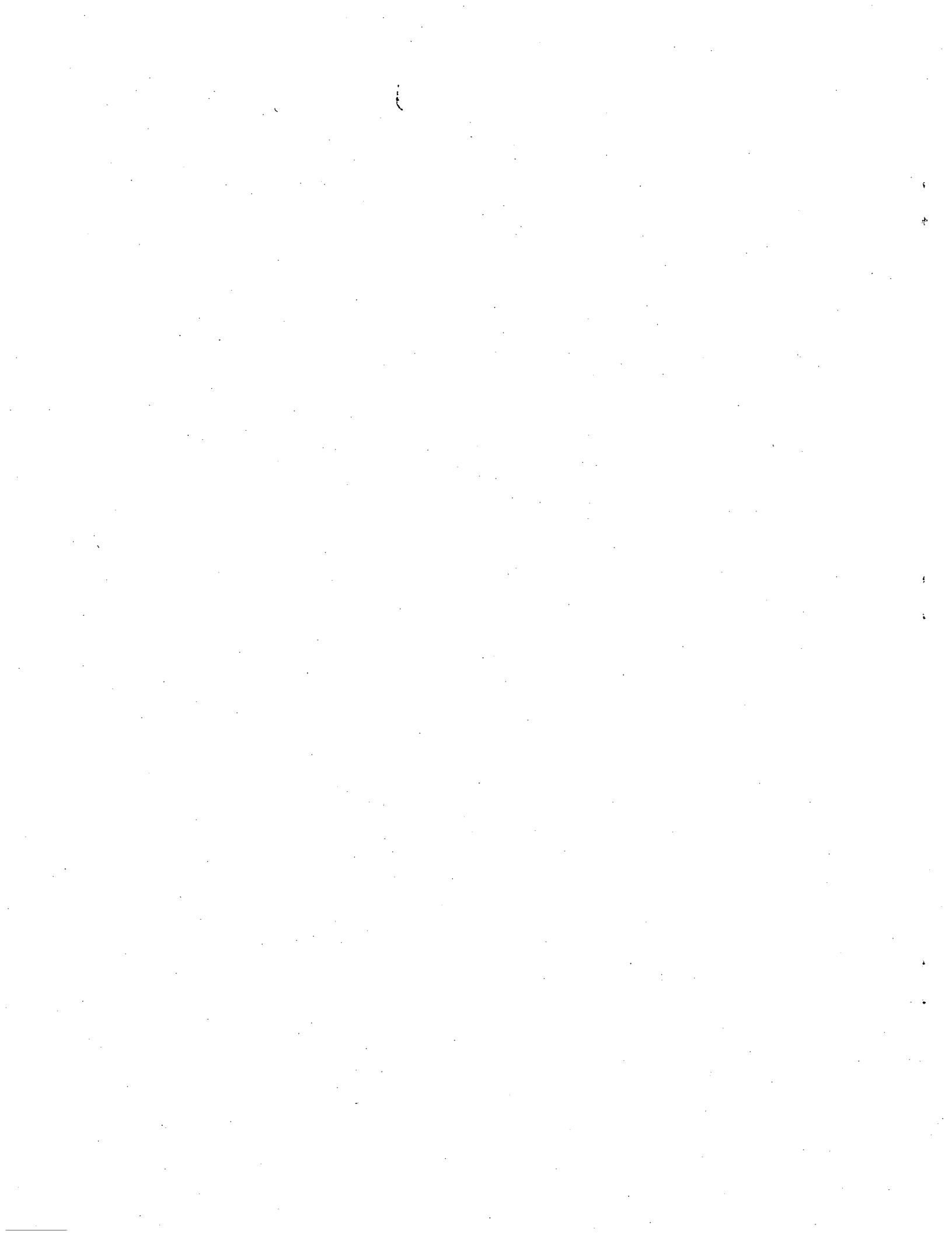
The authors wish to thank Richard Fields of the National Bureau of Standards for stimulating discussions on this paper. The authors also wish to thank C. R. Brinkman, ORNL, and J. P. Gallagher, University of Dayton Research Institute, for all the encouragement they have given to complete this work. Furthermore, the authors appreciate the editing of B. G. Ashdown and the final report preparation of P. J. Dickens.

REFERENCES

1. P. L. Rittenhouse, *Initial Assessment of the Status of HTGR Metallic Structural Materials Technology*, ORNL/TM-4760 (December 1974).
2. C. R. Brinkman et al., *Application of Hastelloy X in Gas-Cooled Reactor Systems*, ORNL/TM-5405 (October 1976).

3. D. A. Jablonski, *Fatigue Behavior of Hastelloy X at Elevated Temperatures in Air, Vacuum, and Oxygen Environments*, Ph.D. Thesis, Massachusetts Institute of Technology, Boston, January 1978.
4. W. R. Corwin, "Subcritical Crack Growth," *Mechanical Properties Test Data for Structural Materials Quart. Prog. Rep. July 31, 1977*, ORNL-5326, pp. 183-88.
5. M. J. Siverns and A. T. Price, "Crack Propagation Under Creep Conditions in a Quenched 2 1/4 Chromium 1 Molybdenum Steel," *Int. J. Fract.* 9: 199 (1973).
6. L. A. James, "Some Preliminary Observations on the Extension of Cracks Under Static Loadings at Elevated Temperatures," *Int. J. Fract.* 8: 347 (1972).
7. G. J. Neale and M. J. Siverns, paper 234/73 in *Int. Conf. Creep and Fatigue in Elevated Temperature Applications*, Institute of Mechanical Engineers, London, 1973.
8. S. Floreen, "The Creep Fracture of Wrought Nickel-Base Alloys by a Fracture Mechanics Approach," *Metall. Trans.* 6A: 1741-49 (1975).
9. R. D. Nicholson and C. L. Fornby, "The Validity of Various Fracture Mechanics Methods at Creep Temperatures," *Int. J. Fract.* 11 (4): 595-604 (1975).
10. J. R. Haigh, "The Mechanics of Macroscopic High Temperature Crack Growth - I: Experiments on Tempered Cr-Mo-V Steel," *Mater. Sci. Eng.* 20: 213-223 (1975).
11. K. M. Nikbin, G. A. Webster, and C. E. Turner, "A Comparison of Methods of Correlating Creep Crack Growth," *4th Int. Conf. Fracture*, Waterloo, Canada, 1977.
12. J. D. Landes and J. A. Begley, *A Fracture Mechanics Approach to Creep Crack Growth*, Westinghouse Scientific Paper 74-1E7-FESGT-P1 (December 1974).
13. D. M. Gilbey, *Measurement of the Length of a Central or Edge Crack in a Sheet of Metal by an Electrical Resistance Method*, TR-66402 (December 1966).
14. R. O. Ritchie, G. G. Garret, and J. F. Knott, "Crack-Growth Monitoring Optimisation of the Electrical Potential Technique Using an Analogue Method," *Int. J. Fract. Mech.* 7: 462 (1971).

15. T. Weerasooriya, *Fatigue Crack Propagation in the Heat-Affected Zone of 2 1/4 Cr-1 Mo Steel and ERNiCr-3 Weldments - Interim Report*, ORNL/TM-6971 (October 1979).
16. S. Taira and R. Ohtani, "Crack Propagation in Creep," pp. 155-81 in *2d Int. Conf. Mechanical Behavior of Materials*, Boston, August 16-20, 1976.
17. R. Koterazawa and T. Mori, "Applicability of Fracture Mechanics Parameters to Crack Propagation Under Creep Conditions," *Trans. ASME Ser. H* 99: 298-305 (1977).
18. M. F. Kanninen et. al., "Elastic-Plastic Fracture Mechanics for Two-Dimensional Stable Crack Growth and Instability Problem," pp. 121-50 in *Elastic-Plastic Fracture*, *Am. Soc. Tech. Mater. Spec. Tech. Publ.* 668, American Society for Testing and Materials, Philadelphia, 1979.



ORNL/TM-7255
 Distribution
 Category UC-77

INTERNAL DISTRIBUTION

- | | |
|------------------------------------|--------------------------------------|
| 1-2. Central Research Library | 40. J. W. McEnerney |
| 3. Document Reference Section | 41. R. K. Nanstad |
| 4-5. Laboratory Records Department | 42. J. C. Ogle |
| 6. Laboratory Records, ORNL RC | 43-49. P. L. Rittenhouse |
| 7. ORNL Patent Section | 50. A. C. Schaffhauser |
| 8. M. K. Booker | 51. G. M. Slaughter |
| 9-18. C. R. Brinkman | 52. J. H. Smith |
| 19. G. R. Gessel | 53-57. J. P. Strizak |
| 20. R. J. Gray | 58. R. W. Swindeman |
| 21. M. L. Grossbeck | 59. F. W. Wiffen |
| 22-24. M. R. Hill | 60. M. H. Yoo |
| 25. H. Inouye | 61. A. L. Bement, Jr. (Consultant) |
| 26-35. P. R. Kasten | 62. W. R. Hibbard, Jr. (Consultant) |
| 36. J. F. King | 63. E. H. Kottcamp, Jr. (Consultant) |
| 37. J. J. Kurtz | 64. Alan Lawley (Consultant) |
| 38. C. T. Liu | 65. M. J. Mayfield (Consultant) |
| 39. H. E. McCoy | 66. J. T. Stringer (Consultant) |

EXTERNAL DISTRIBUTION

- 67-68. DOE, DIVISION OF NUCLEAR POWER DEVELOPMENT, Washington, DC 20545

Director
 G. A. Newby

69. SAN-DEVELOPMENT, SAN DIEGO AREA OFFICE, P. O. Box 81325, San Diego,
 CA 92138

Senior Program Coordinator

70. DOE, SAN FRANCISCO OPERATIONS OFFICE, 1333 Broadway, Wells Fargo
 Building, Oakland, CA 94612

Manager

- 71-72. DOE, OAK RIDGE OPERATIONS OFFICE, P. O. Box E, Oak Ridge, TN
 37830

Office of Assistant Manager, Energy Research and Development
 Director, Nuclear Research and Development Division

73-238. DOE, TECHNICAL INFORMATION CENTER, Office of Information
Services, P. O. Box 62, Oak Ridge, TN 37830

For distribution as shown in TID-4500 Distribution
Category, UC-77 (Gas Cooled Reactor Technology).